JOURNAL OF GEOPHYSICAL RESEARCH, VOL. 99, NO. B3, PAGES 4741–4760, MARCH 10, 1994

Volcanic and hydrothermal processes associated with a recent phase of seafloor spreading at the northern Cleft segment: Juan de Fuca Ridge

R. W. Embley

Pacific Marine Environmental Laboratory, NOAA, Hatfield Marine Science Center, Newport, Oregon

W. W. Chadwick, Jr.

Oregon State University, Cooperative Institute for Marine Resources Studies
Hatfield Marine Science Center, Newport, Oregon

Abstract. The northern portion of the Cleft segment, which is the southernmost segment of the Juan de Fuca Ridge, is the site of a seafloor spreading episode during the mid-1980s that was originally discovered by the occurrence of anomalous hydrothermal bursts (megaplumes) and later documented by seafloor mapping of new pillow mounds (NPM) that were erupted. Several field seasons of investigations using sidescan sonar, a deep-tow camera system, and the submersible *Alvin* reveal that about 30 km of the ridge crest is hydrothermally active and/or has experienced recent volcanic and tectonic activity associated with this episode. The most intense hydrothermal activity within this area and all the known high-temperature vents lie along a fissure from which a young sheet flow (YSF) erupted. Extinct chimneys located within 100–200 m on either side of the fissure system represent an older (>100 years) and probably less intense, hydrothermal regime. The bathymetry and the morphology of the YSF suggest that this eruption occurred over a 1–2 km section of the fissure system that forms its eastern boundary and that it flowed to the south. Fields of lava pillars concentrated at the margins of the YSF where lava probably formed when the lava stagnated near the edges of the flow. A comparison of sidescan data sets collected in 1982 and 1987 implies that the YSF was erupted at least 7 months prior to the NPM, consistent with analysis of bottom photographs that suggests that the eruptions of the YSF and NPM were only separated by a few years. The low hydrothermal flux over the NPM relative to the YSF suggests a rapidly cooled underlying heat source beneath the former. We propose that the NPM were erupted from a dike or dikes injected laterally to the north from a magma body lying beneath the YSF. Recent evidence of a decrease in the intensity of the overlying hydrothermal plumes suggests that the system is continuing to cool down.

Introduction

In 1986, an anomalously large hydrothermal plume was discovered over the northern Cleft segment of the southern Juan de Fuca Ridge (Figures 1 and 2) [*Baker et al.*, 1987]. The "megaplume," as it came to be known, contained a thermal discharge of about 10^{16}–10^{17} J and had a distinct hydrothermal chemical signature [*Baker et al.*, 1987, 1989]. Another megaplume (Megaplume II) was discovered overlying the Vance segment about 40 km north of the first megaplume in 1987. The rise height and size of the megaplumes strongly imply that they were transitory features related to the sudden breaching of a hydrothermal reservoir, probably a seafloor rifting event [*Baker et al.*, 1989]. Although the source of the megaplumes could not be determined during the water column surveys, the occurrence of less intense, deeper, and more "steady state" hydrothermal plumes over the adjacent ridge crest suggested a likely source area. An investigation of this area using sidescan sonar, a towed-camera, continued water column surveys, and submersible dives followed over the next several field seasons. The purpose of the surveys was to define the volcanic, tectonic, and hydrothermal characteristics of the ridge crest from which the megaplumes originated in order to constrain the possible source mechanisms. The most significant result of this work was the discovery that a volcanic eruption occurred at this site between 1983 and 1987, strongly implying a link to the megaplumes [*Embley et al.*, 1990a; *Chadwick et al.*, 1991; *Fox et al.*, 1992]. *Embley et al.* [1991] presented an initial description of the geology of this area, but *Chadwick and Embley* [this issue] and we (1) describe the geologic setting of the southern Juan de Fuca Ridge, (2) present detailed observations of the hydrothermal, tectonic, and volcanic relationships along the northern Cleft segment, and (3) present an interpretation of the sequence of events that took place in this area during the past decade and the implications for processes on ridge crests.

Paper number 93JB02038.
0148-0227/94/93JB-02038$05.00

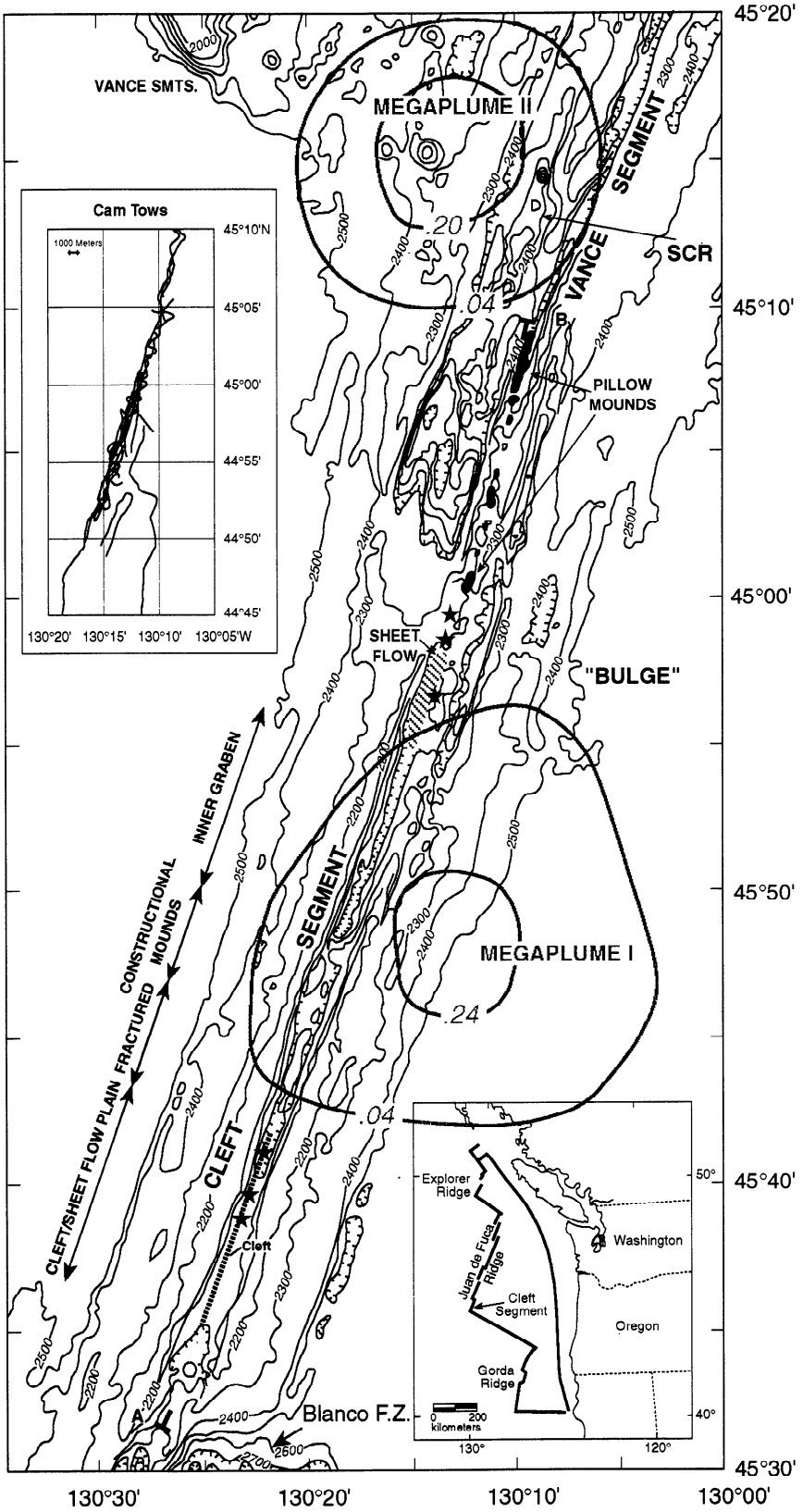

Figure 1. Simplified Sea Beam map of portion of area of Plate 1 showing features discussed in text. Contour interval is 100 m except for the axial valley, where it is 20 m. Temperature anomaly contours of megaplumes are from *Baker et al.* [1989]. Solid line from 44°35'N to 44°42'N is location of cleft [after *U.S. Geological Survey Juan de Fuca Study Group*, 1986]. Locations of new pillow mounds and young sheet flows are indicated. Stars show location of high-temperature vents. SCR is Split Cone Ridge. Index map at lower right shows location of mapped area. Inset at upper left shows locations of NOAA towed camera tracks made between 1987 and 1991. A-B shows location of along-axis bathymetric profile shown on Figure 2.

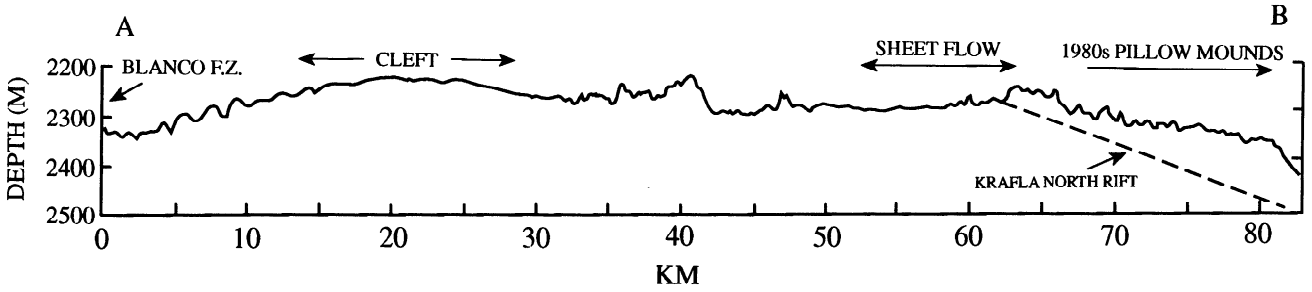

Figure 2. Along-axis bathymetric profile of Cleft segment (A-B) constructed from 100-m grid. Location shown in Figure 1. Dashed line shows gradient of portion of north rift zone of the Krafla central volcano, Iceland.

Methods

This study presents an interweaving of four types of data, each with a different resolution: (1) Sea Beam bathymetry, (2) SeaMARC I sidescan sonar backscatter imagery, (3) towed-camera photogeology and microbathymetry, and (4) submersible observations and sampling. A brief description of the methods used in collecting and processing these data follows.

Sea Beam

The original Sea Beam data set was collected using LORAN-C navigation during 1981–1984 from the NOAA ship *Surveyor*. Data from additional surveys by the *Atlantis II* in 1987 and the NOAA ship *Discoverer* in 1990 and 1992 extended coverage to the flanks of the ridge and corrected the bathymetry for depth changes caused by the volcanic eruption during the mid 1980s at the northern end of the Cleft segment (Figure 2) [*Fox et al.*, 1992]. The operational characteristics of the Sea Beam system have been described by *Renard and Allenou* [1979], and *de Moustier and Kleinrock* [1986], and the processing techniques used to produce the maps in this Special Section are described by *Embley et al.* [1990a]. The map coordinate system was obtained by applying a geodetic corrector to the original LORAN-C navigation (but note that LORAN-C was used in previously published maps for this area of *Chadwick et al.* [1991], *Embley et al.* [1991], and *Fox et al.* [1992].

SeaMARC Sidescan

A single 5-km swath of SeaMARC I sidescan sonar (30 kHz) of the neovolcanic zone over the Juan de Fuca Ridge was collected in 1982 [*Kappel and Ryan*, 1986; *Kappel and Normark*, 1987]. Unfortunately, the digital logging system on this cruise was inoperative, so only analog records were obtained. In August 1987 the NOAA ship *Discoverer* resurveyed the axial valley of the Cleft segment with a deep-towed SeaMARC I sonar, and three overlapping 2-km-wide swaths of digital sidescan data were obtained along the entire segment between 44°28′N and 45°02′N. The initial processing techniques used for this data are described by *Appelgate* [1990].

Towed Camera

A towed-camera system designed and constructed at the Pacific Marine Environmental Laboratory (PMEL) was used to collect the photogeologic and microbathymetry data. Data from the NOAA PMEL camera system include pressure depth, altitude, light attenuation, temperature, salinity, 35-mm photographs, and real-time black and white video. The camera was flown by monitoring the real-time video, the altimeter, and an obstacle avoidance sonar. Because the repetition rate of the still camera can be adjusted from the surface, the timing interval of the photographs varies from tow to tow, depending on the complexity of the geology, tow speed, etc. The 35-mm photographs are analyzed according to the general scheme described by *Fox et al.* [1988] and *Embley et al.* [1990a]. These merged data can then be plotted as map views or cross sections for analysis. Most of the towed-camera data collected for this study were used long-baseline acoustic transponder navigation. The crossing errors are estimated at about 10–20 m for data collected during a given field season.

Alvin Submersible Dives

Forty-two *Alvin* dives have been made along the Cleft segment between 44°54′N and 45°10′N during three expeditions in 1988, 1990, and 1991. About half of the dives concentrated on vent fluid sampling and conducting experiments on the dynamics of buoyant hydrothermal plumes and did not provide extensive geologic observations. The 1988 dive series was severely hampered by the absence of a gyro compass and poor navigation. An in-sub navigation system became operational about halfway through the 1990 dive series and on most of these dives, the relative position of the submersible is known to less than 5 m. The *Alvin* data were processed in a similar manner to the towed-camera data.

Cleft Segment: Overview

The morphology of the southern Juan de Fuca Ridge has been generally described by *Embley et al.* [1983], *Kappel and Ryan* [1986], and *Kappel and Normark* [1987]. The Cleft segment (Figure 1 and Plate 1) is the southernmost discrete spreading segment of the Juan de Fuca Ridge, beginning at 44°27′N at its intersection with the Blanco Fracture Zone and ending in an overlapping relationship with the Vance segment at or slightly north of 45°10′N [*Kappel and Ryan*, 1986; *Murphy and Embley*, 1988; *Johnson and Holmes*, 1989; *Embley et al.*, 1991]. The along-axis high is at 44°38′N and from here seafloor depth drops off rapidly to the south into the Blanco Fracture Zone and more gradually to the north, dropping less than 100 m over the first 50 km and then another 100 m in the next 15 km along a pillow mound ridge (Plate 1 and Figures 1 and 2). Although the present along-axis high point occurs at 44°38′N, the smoother and shallower relief of the flanks of the ridge between about 44°50′N and

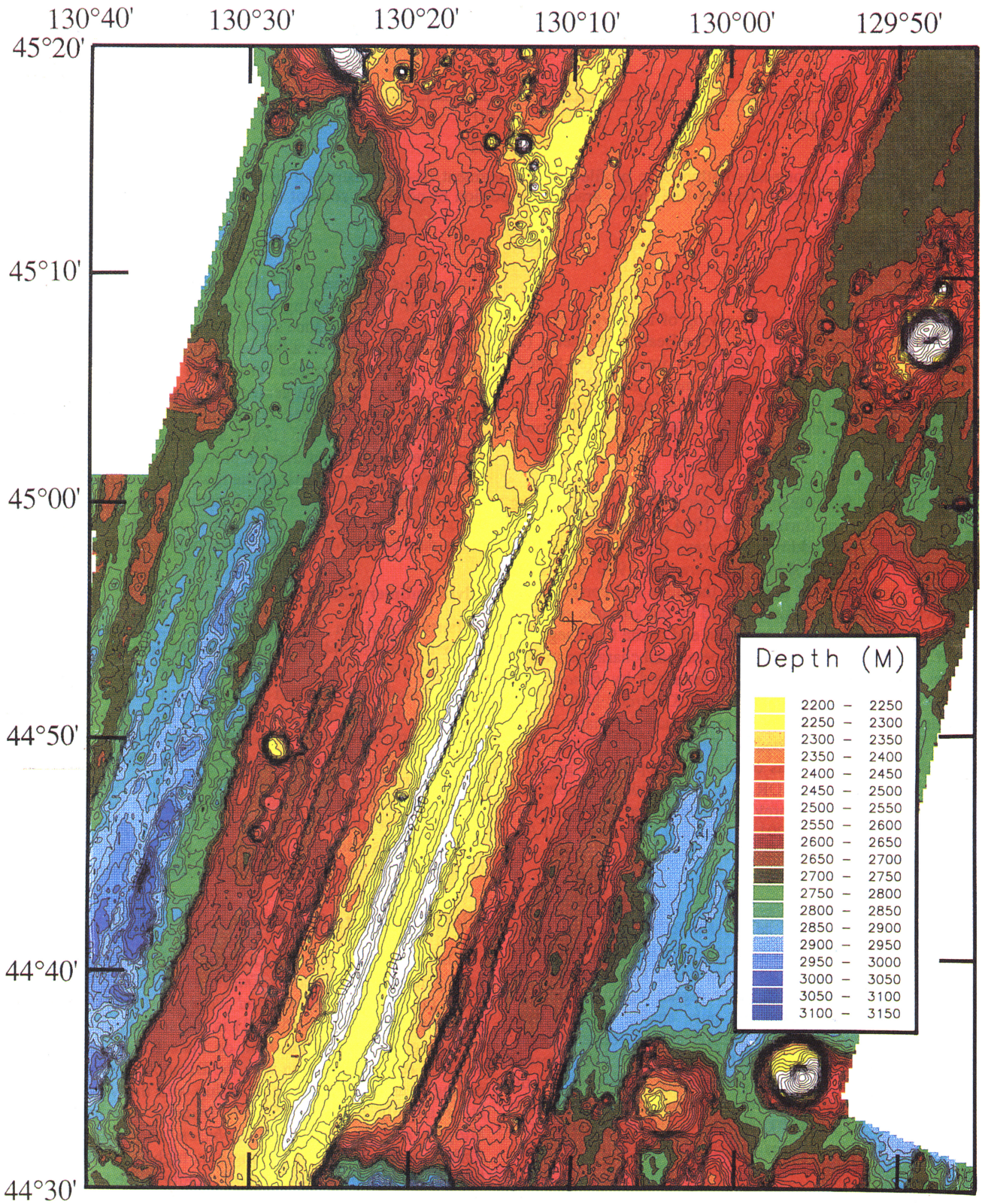

Plate 1. Sea Beam bathymetric map of southern Juan de Fuca Ridge. Track line spacing approximately 1.8 km to produce nearly 100% coverage. Contour interval is 20 m, color interval is 50 m. Grid spacing is 100 m.

45°02′N (Figure 1) implies a higher average rate of extrusive volcanism versus tectonism along the northern third of the segment over the past few hundred thousand years.

The morphology of the Cleft segment varies along its 80-km length (Plate 1 and Figure 2). The segment's name is derived from the presence of a nearly continuous cleft that is 10 km in length, 30 to 50 m in width, and 20 m in depth, extending along the segment's along-axis high from about 44°35′N to 44°44′N within a broad, 3-km-wide axial valley. This cleft is centered along an untectonized lava plain that extends 15 km along the axis from 44°35′N to 44°43′N. High-temperature vents are found at three locations along the cleft (Figure 1), probably the sites of eruptive centers that fed the lava plain sheet flows [*U.S. Geological Survey (USGS) Juan de Fuca Study Group*, 1986].

North of the smooth lava plain, beginning at about 44°44′N, the axial valley of the Cleft segment deepens and becomes more fissured, although a zone of relatively untectonized constructional volcanic terrain covers the axial valley from 44°46′N to 44°49′N. Between 44°49′N and 44°55′N, a distinct 500-m-wide inner graben is present (Plates 1 and 2 and Figures 2 and 3). From 44°54′N to 44°59′N, a series of small constructional cones and ridges lies on a line roughly bisecting the neovolcanic zone. North of here, the neovolcanic zone can be traced along the crest of a gentle volcanic ridge to about 45°10′N (Plate 1 and Figure 1). This ridge overlaps the Vance axial valley by about 18 km and curves slightly to the west. The southern portion of the Vance axial valley, which is distinctly wider and deeper than the Cleft axial valley, has a central volcanic constructional ridge (split cone ridge or SCR) that overlaps with and curves toward the Cleft neovolcanic ridge, in the style of the overlapping spreading centers of the East Pacific Rise [*Macdonald et al.*, 1984].

Northern Cleft Segment: Morphology and Volcanology

The termination of the morphologically distinct inner graben occurs at 44°55.5′N (Plate 2 and Figures 3a and 3b). This sudden change in structure is probably a fourth-order discontinuity as defined by *Macdonald et al.* [1988]. The western boundary fault continues north to about 45°00′N where it becomes buried by younger flows. North of 44°54′N (Plate 2) the eastern boundary fault becomes a low relief feature only about 20 m high. The 100-m relief trough and ridge on the east side of the axial valley (ETR on Figure 3b) is not the eastern boundary fault of the present axial valley but a slightly older feature. Between 44°56′ and 45°01′N, the neovolcanic zone is centered between the 100-m relief western boundary fault and the poorly defined continuation of the eastern boundary fault (Plate 2 and Figure 3).

Within the axial valley north of 44°55′N, several types of constructional features are present. Bisecting the axial valley from 44°55.7′N to 44°59.5′N is a string of mounds (marked age 2 on Figure 3b on a relative age scale in which age 1 is youngest and age 4 the oldest) which are composed primarily of pillow lavas with a few fissures cutting through them (Figure 3a). The lava flows erupted during the 1980s (marked age 1 on Figure 3b and henceforth designated the new pillow mounds (NPM) are only barely differentiable on sidescan sonar records from the age 2 mounds by the complete lack of fissures on the NPM (confirmed by towed camera and submersible observations). Surrounding the constructional mounds are areas of flat, smooth seafloor. These are composed primarily of sheet flows. One particularly young sheet flow (YSF) that appears to be almost as young as the NPM (described in detail below) lies primarily west of the pillow mounds and extends south to the northern portion of the inner graben at 44°55′N (Plate 2 and Figure 3b).

Another type of constructional feature is somewhat enigmatic. These are ridges lying along the northwestern portion of the axial valley (north of 44°59′N and labeled LRR on Figure 3b, for Lava Rise Ridge) which are covered primarily by jumbled sheet flows. Narrow, 020°N trending fractures penetrate the 40-m high east flank of one ridge, and several 5- to 10-m wide, noneruptive fractures are found along the top (Figures 5a and 5b). Observations from an *Alvin* dive that followed one of these cracks for several hundred meters revealed that the jumbled flows cap massive, columnar-jointed units. The large fractures located near the top of the steep flanks of the ridge resemble "lava inflation clefts" [*Walker*, 1991]. The LRR appears to be a large lava inflation feature caused either by the continued introduction of lava into a flow lobe during the solidification of the outer crust or by later intrusion from below. Similar features have been described in Hawaii [*Walker*, 1991], on Axial Volcano, Juan de Fuca Ridge [*Appelgate and Embley*, 1992], and near the Kane Fracture Zone on the Mid-Atlantic Ridge [*Humphris et al.*, 1990].

The NPM and YSF are both superimposed on distinctly older flows. Their young age, which is evident from their 0–5% sediment cover and vitreous luster (Plates 3a and 4h), allows the contacts between young and old lavas to be easily mapped with bottom photography. The young flows are morphologically distinct from each other. The YSF consists primarily of a mixture of ropy, lineated and lobate flows covering an area of about 3.5 km^2 between 44°55.5′N and 44°59.5′N. North of the YSF, from 45°01′N to about 45°10′N, the NPM consist of a string of discontinuous pillow lava mounds covering up to several square kilometers along the crest of the ridge that overlaps with the Vance axial valley [*Chadwick and Embley*, this issue] (Figure 1). Repeat Sea Beam surveys have shown that these mounds were erupted between 1983 and 1987 [*Embley et al.*, 1990b; *Chadwick et al.*, 1991; *Fox et al.*, 1992]. A comparison of bottom photographs between the YPM and YSF shows no distinguishable difference in sediment cover or reflective properties, and therefore we interpret the YSF to be only years to decades old. The young lava flows of the northern Cleft segment are distinctly younger than flows found elsewhere on the segment, including those forming the lava plain to the south, which *Normark et al.* [1983] estimated to be less than a few hundred years old.

The boundary of the young sheet flow is, for the most part, not distinguishable on sidescan imagery (Figures 3 and 5), because the edge of the YSF is similar in morphology to the surrounding older flows (e.g., southern boundary) and the difference in sediment cover between the young and older flows is not great enough to cause a significant change in backscatter intensity. However, there are distinct backscatter differences between different flow types within the YSF. The most striking differences occur between areas of very flat, lineated lavas characterized by low backscatter and areas of chaotic, jumbled, or collapsed sheet flows characterized by high backscatter (note area between 44°57′ to 58′N and 130°13′ to 14′W) (Figure 3a). Lobate flows appear to be characterized by an intermediate level of backscatter.

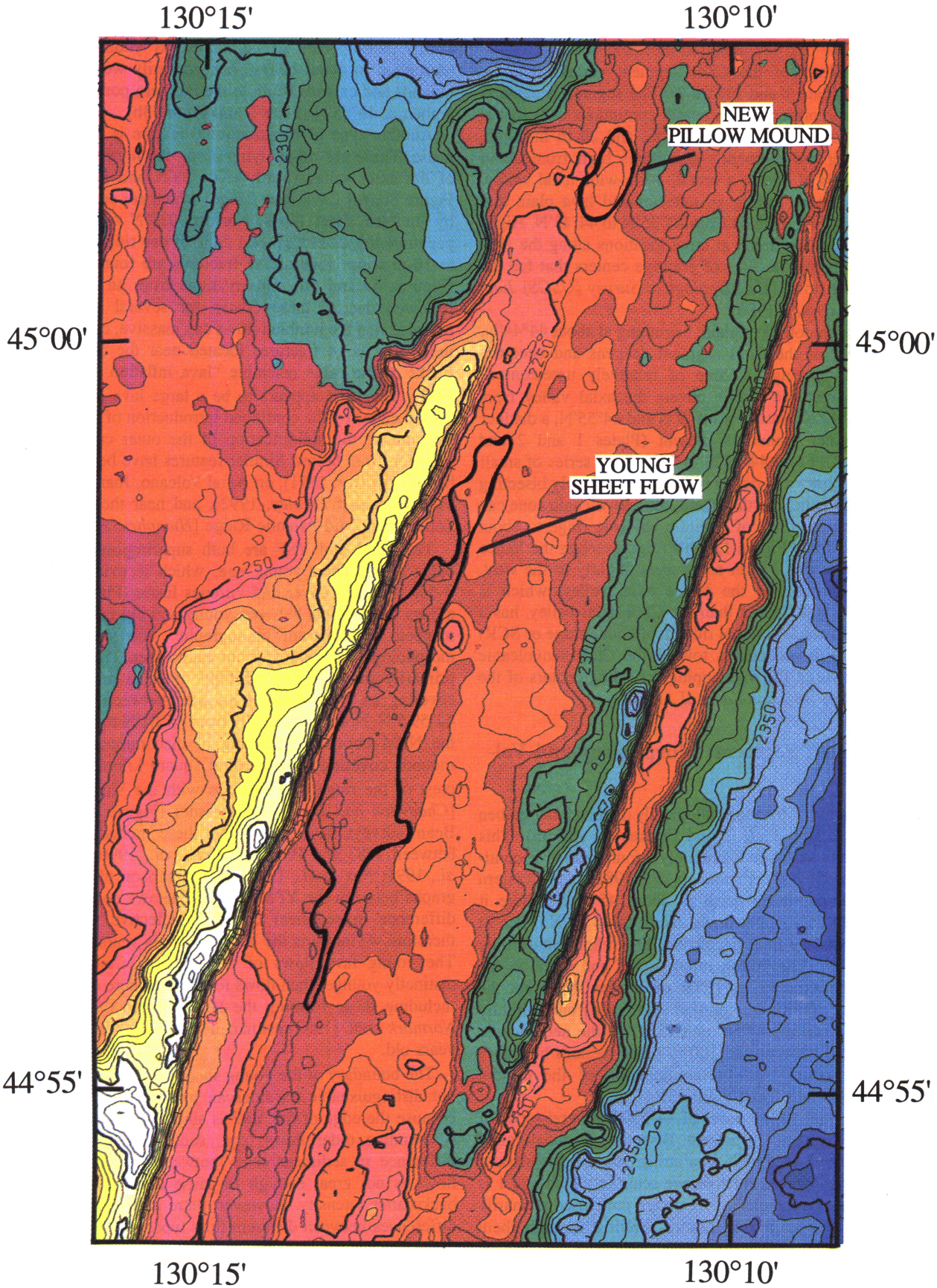

Plate 2. Sea Beam bathymetry of northern Cleft segment. Contour interval is 5 m and color interval is 20 m. Raw Sea Beam depth is corrected to *Alvin* depths for this area (15 m subtracted from raw Sea Beam data). Bold line is outline of young sheet flow (YSF).

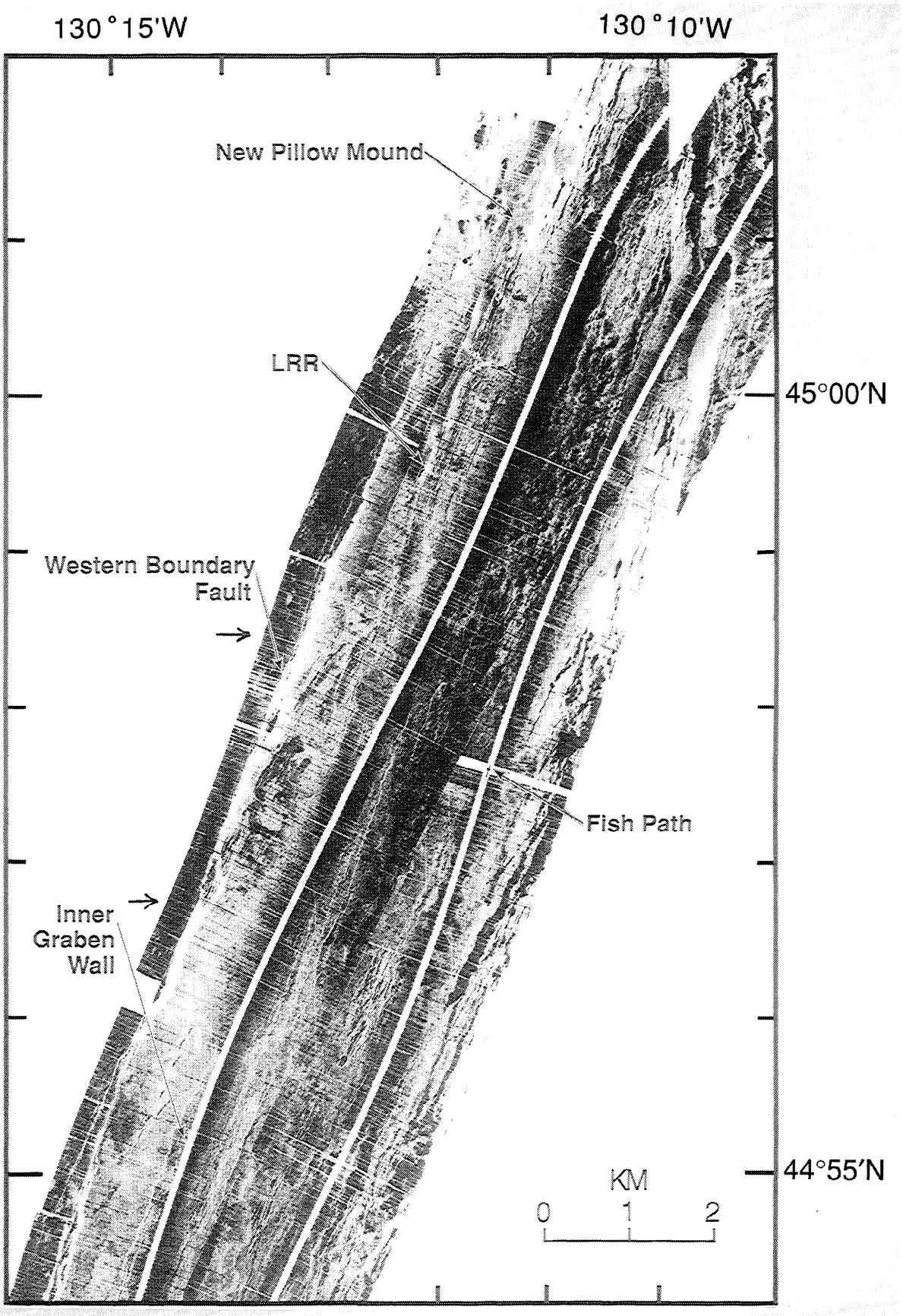

Figure 3a. Mosaic of three SeaMARC 1A (30 kHz) sidescan swaths of northern Cleft, the same area as Plate 2 and Figure 3b (opposite). White ribbons are center beam of sidescan. White is high reflectivity, and black is low reflectivity or shadows. Each swath is 1 km on each side with 1048 pixels across total swath. See Figure 3b for full names of abbreviations. Approximate latitudinal limits of sidescan swaths shown in Figure 4 are indicated by arrows.

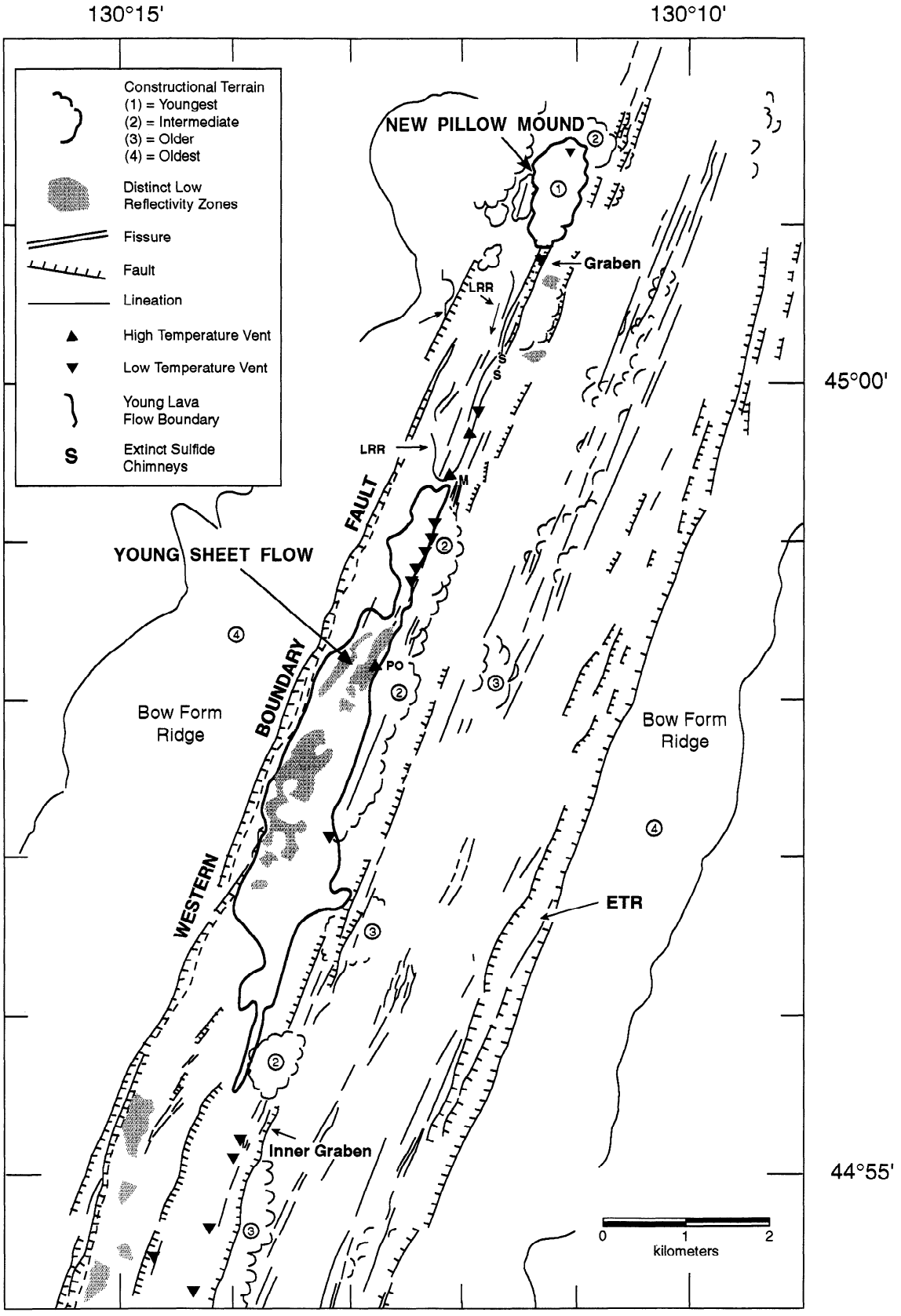

Figure 3b. Interpretative map of sidescan in Figure 3a for northern Cleft segment. Roughly the same area as Plate 2 and Figure 3a. Features outside of Cleft axial valley based on Sea Beam map (Plate 2). Bold line is outline of young sheet flow (YSF). PO is Pipe Organ Vent, M is Monolith Vent, ETR is Eastern Trough, and LRR is Lava Rise Ridge. S indicates location of extinct sulfide chimney fields located north or south of area covered by Figure 5.

With this understanding of the origin of the backscatter contrasts at this site, we compared sidescan sonar data collected over the same portion of the YSF in 1982 and 1987 (Figure 4) to see if the YSF is present in both. The 1982 data were of significantly lower quality (the ship was turning at the time and only analogue data were available), but the same backscatter patterns are apparent. Therefore we conclude that the YSF was erupted prior to October 1982, at least 7 months before the NPM eruption.

Near the northern end of the YSF there is a topographic constriction where lava flowed through a constriction at 44°58.1′N (Figure 6e and Figure 5a). The upper surface of the YSF is nearly flat, both north and south of the constriction, but it is about 12 m lower on the south side. The original flow top (before collapse) is at 2263 m at the north end of the flow, at 2273 m at the constriction, and at 2275 m south of the constriction (Figure 6). Another contrast is that the height of the lava pillars within the collapse areas is typically 1 m north of the constriction but 5 m south of it. However, on any given east-west cross section the tops of the pillars are at the same depth to within less than a meter, representing the original surface of the flow. This is evidence that much of the YSF lava was erupted at the northern end of the flow and quickly flowed south through the constriction where it then spread out and ponded in a broad shallow depression between the age 2 pillow mounds and the western boundary fault (Plate 2 and Figure 3).

This sheet flow consists of a wide range of lava morphologies because the interior of the flow has drained out and is collapsed in many areas. The original upper surface of the flow is lobate in morphology, where it is preserved at the flow edges and on the top of the pillars (Plate 3a). The collapse areas are floored by lineated, ropy flows, and jumbled sheet flows (Plates 3a–3e). South of 44°58′N, the lava onlaps the base of the talus slope of the western bounding fault.

The eruptive fissure for the YSF is interpreted to be a NE-SW (~020°) trending fissure system along the western shoulder of the age 2 pillow mounds, and it is along this trend that most of the high-temperature and low-temperature diffuse vents are concentrated [*Embley et al.*, 1991] (Figures 3b and 5a). This en echelon fissure system along the eastern edge of the YSF is most continuous north of 44°58.5′N. Classic drainback features are seen along the fissure (particularly north of the Cavern Vent at 44°59′N (Figure 5a)), including draped sheets and drainback cavities at the lip of the fissure (Plates 3f–3i). In some places, primarily between Cavern and Marker 4 and at the Tripod vent (Figure 5a), fissures cut through the young sheet flows, indicating some posteruptive extension. There is only minimal vertical offset (~1–2 m) (Figure 6d). The fissure system is generally within the YSF, except at 44°58.3′N (Figure 5a) where it cuts through a section of the age 2 pillow mound.

Zones of lava pillars and "shelly" lobate flows [*Embley et al.*, 1990a] are found along the edges of the flow, predominantly on the eastern side adjacent to the hydrothermally active fissure system (Figures 6b–6f) but also on the western side of the sheet flow near the wall (Figure 6f). NE-SW trending lineated lava flows are found in the interior of the YSF, along with small pushup ridges (Plate 3e), which usually have a long axis perpendicular to the lineations. Numerous examples of transitions from lineated to ropy and whorly pahoehoe-like flow surfaces show that the lineated flow surface is created by flow of lava in a southwesterly direction parallel to the lineations (e.g., Plate 3c). The lower flow surface postdates the formation of the pillars since rubble from broken pillars and collapsed roof sections is commonly found on the lower surface.

North Cleft Segment: Hydrothermal Vents

A 6-year time series of CTD "tow-yos" along the southern Juan de Fuca Ridge has shown that the Cleft segment is producing hydrothermal plumes that originate from two distinct sources [*Baker*, this issue]. The southern vent fields include several black smoker sites lying between 44°38′N and 44°41.5′N (Figure 1) within the "cleft" [*U.S. Geological Survey Juan de Fuca Study Group*, 1986; *Normark et al.*, 1987]. As discussed above, the northern vent sites lie between 44°53′N and 45°03′N, where towed camera and submersible observations reveal extensive diffuse venting (<60°C) and several black smokers, including Pipe Organ, Monolith, and Fountain vents (Figure 5a). There is no unequivocal photographic evidence of active venting (e.g., chemosynthetic biological communities) along the neovolcanic zone between the southern and northern sites, although some small yellow/orange deposits and small temperature anomalies have been recorded (by NOAA and USGS camera systems) [*Kappel and Normark*, 1988; R.W. Embley, unpublished data, 1989]. However, there has not been any detailed mapping in this region (Figure 1, inset).

The most extensive venting on the northern Cleft segment occurs along the fissure system at the eastern boundary of, and within about 5 km north and south of, the YSF. North of 44°59.5′N, venting becomes less vigorous and more widely spaced and no active venting has been found north of about 45°04′N.

The southernmost venting is within the inner graben between 44°53′N and 44°55.3′N and consists of low-temperature vents. The densest concentration of vents occurs within a shallow trough within 100 m of the base of the eastern side of the inner graben (Figure 6i and Plate 4a). Sporadic venting can be followed for hundreds of meters along fractures and lava push-ups identifiable by characteristic white "staining" on broken lava surfaces (Plate 4b). Two isolated inactive sulfide chimneys occur about 100 m east of the active vents (Plate 4c). The extent of venting along the west side of the graben is less well known, because of the difficulty of maneuvering a towed camera near the steep wall, but some vents are confirmed here by several temperature anomalies and photographs.

The (known) high-temperature vents and the highest density of diffuse vents along the northern Cleft segment occur along the fissure system on the east side of the YSF and along its continuation immediately to the north (Figure 5a). Across any particular cross section, all the venting is located either within the main fissure system, or within a few tens of meters from the fissure. Although no high-temperature vents were found during the first submersible dives at the northern Cleft site in 1988, extensive low-temperature diffuse vents (up to 60°C) were mapped along several hundred meters of the main fissure system. Bacterial mats were extensive, and there were also thousands of globules of mucous-like polymers associated with the mats [*Milligan and Tunnicliffe*, this issue], reminiscent of the extensive bacterial floccules at 9–10°N found immediately after an eruption in 1991 [*Haymon et al.*, 1993]. At the Tripod Vent (named for a large tripod at the site), the 1988 dives

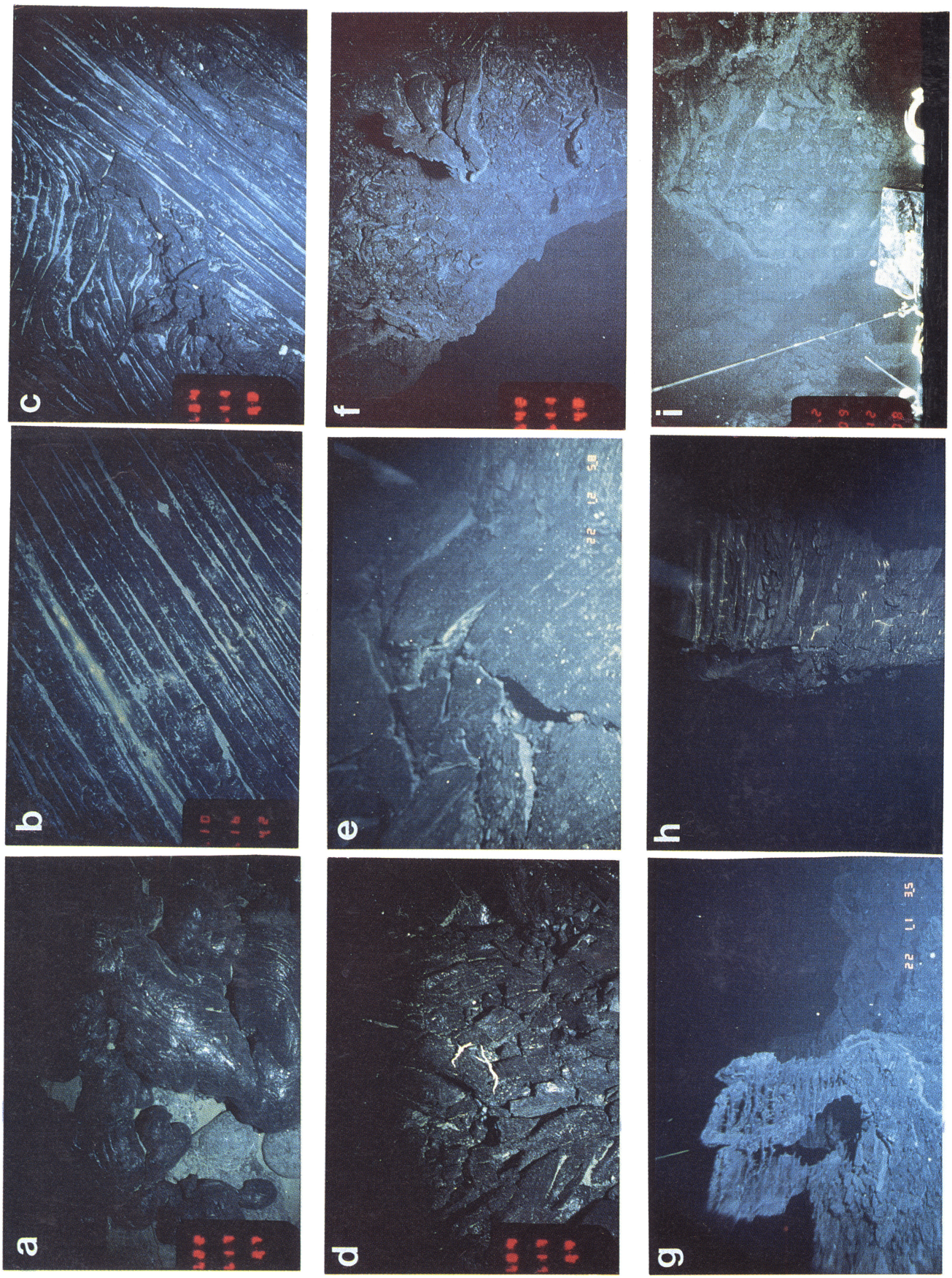
a
b
c
d
e
f
g
h
i

documented extensive venting through posteruptive fractures in the glassy lava. At that time there was only a small amount of hydrothermal sediment (Plate 4d). By 1990, however, the lavas at this site had been extensively covered with iron-rich sediment [*Massoth et al.*, this issue; *Butterfield and Massoth.*, this issue] (Plate 4e), the maximum vent fluid temperature had decreased from 60°C to 25°C, and the vent fauna had drastically decreased in numbers. On a subsequent visit in 1991, the venting had become so diffuse that it was no longer possible to obtain a vent fluid sample for analysis.

The vents along the eastern edge of the YSF north of the Tripod site are all diffuse vents with maximum temperatures <60°C and most are <30°C. Between the Marker 4 vent and the Cavern vent, all the vents lie along a fissure system that was traversed by *Alvin* in 1988, 1990, and 1991 (Figure 4f). Two or three closely spaced fissures occur in this area, but only one is actively venting on any cross section.

The Pipe Organ vent is the only known high-temperature vent located along the eastern edge of the YSF. This vent, about 100 m south of the Tripod Vent, consists of six to 10 narrow, fragile, pipelike chimneys venting water up to 260°C (Plate 4g). The chimney field is entirely confined within and emerging from the YSF (and so postdates it) and has no substantive sulfide mound surrounding it [*Koski et al.*, this issue]. It lies about 10 m west of the contact with the age 2 pillow mounds. The fluids sampled from the Pipe Organ vents have high iron-manganese ratios that distinguish it from the high-temperature vents north of the sheet flow [*Butterfield and Massoth*, this issue].

The Monolith vent is the most robust of the high-temperature vents found at the north Cleft segment. It lies just north of the YSF where the main fissure system cuts into the base of the LRR (Figure 5). The Monolith is an agglomeration of chimneys that is about 4 m in diameter and 5 m high, and vents water up to 327°C and immediately west of Monolith is the steep, east facing slope of the LRR. North of Monolith, the active fissure cuts across the slope of the LRR (Figure 5). Several smaller vents lie on the same trend within along the fissure to the north. The morphology and mineralogy of the Monolith vent has led *Koski et al.* [this issue] to propose that it is an older, lower-temperature structure that has been rejuvenated by an increased flow rate and temperature (possibly from the megaplume/NPM eruption events). Another, smaller high-temperature vent (Fountain vent) is found about 600 m north of Monolith along the 020° trend. This is the only one of the three active high-temperature vents that has an extensive biological community associated with it. Several diffuse vents and groups of extinct sulfide chimneys are found along the same trend within a few hundred meters north of the Fountain vent (Figure 3b).

Abundant yellowish deposits (Plate 4h), sometimes exceeding ~1×10^3 m^2 in area, and whitish stains coat the YSF in places (Figure 4h). These have not been extensively sampled, but some of them contain elemental sulfur, boehmite and Fe-Si hydroxides. Since most of these sample locations are not in presently active venting areas, they probably formed near the time the YSF erupted. This material may represent products deposited by diffuse venting from an immature hydrothermal system like that observed after the recent eruption on the EPR [*Haymon et al.*, 1993]. Also, the presence of the mineral boehmite [*Howard and Fisk*, 1988; I. Jonasson, personal communication, 1989] on some of the fractures in areas not presently venting indicates that high-temperature venting had at one time been considerably more widespread than during the first submersible visit in 1988.

Several dozen extinct chimneys have been mapped within 100–200 m of the primary fissure system. In some places they are found at the contact between the young sheet flow and older lavas. These chimneys commonly form chains that parallel the primary fissure system for short distances. At two sites the young lava is observed to directly onlap a chimney (Plate 4i). At another site a chimney had been broken by a fracture that cut through the chimney. Most of these older chimneys are characterized by a high silica content and a dominant pyritic mineralogy, implying a formation temperature below 200°C [*Koski et al.*, this issue]. These older chimneys represent a pre-YSF, less robust phase of hydrothermalism.

Discussion

Sequence of Events

The detailed observations presented above offer some important clues about the recent sequence of events at the north Cleft segment.

Pre-YSF eruptions. Little is known of specific events before the eruption of the YSF, but the axis of intrusion and extrusion was apparently 100–200 m east of the YSF eruptive vents, judging from the locations of Age 2 pillow mounds and associated fissure swarms (Figs. 3 and 5). The age of the Age 2 pillow mounds is unknown, but judging from the amount of sediment cover, some of these mounds probably erupted within the past few hundred years. The older chimneys probably formed after the eruption of these mounds and the older sheet and lobate flows on their west side. One of these chimneys has been dated at >100 years by Pb^{210} [*Koski et al.*, this issue].

YSF and NPM eruptions. Both the YSF and NPM eruptions were fed from long line sources; dikes intruded along different parts of the same fissure system [*Embley et al.*, 1991; *Chadwick and Embley*, this issue]. However, there is evidence that the YSF and NPM erupted during two separate events probably separated by only a decade or less. The lava flows produced by these eruptions differ dramatically in their morphology, indicating that the YSF was erupted at a much higher rate than the NPM [*Griffiths and Fink*, 1992].

The north-to-south topographic gradient and the NE-SW

Plate 3. Photographs of northern Cleft geologic features. ALVBC, *Alvin* bow camera; ALVHH, *Alvin* handheld camera; TC, towed camera (approximate scale across bottom of photo). (a) (TC) Contact of young sheet flow with older lobate flows (4 m). (b) (TC) Lineated sheet flow with low-temperature hydrothermal deposits (4 m). (c) (TC) Transition from young lineated sheet flow to ropy and jumbled flows (5 m). (d) (TC) Young Jumbled flow (4 m). (e) (ALVHH) Pushup structure in young sheet flow (3 m). (f) (TC) Looking down on young fissure with remains of collapsed and drained-back lobate flow at edge (5 m). (g) (ALVHH) Lava spires with multiple "bath-tub ring" shelves at western edge of fissure (3 m). (h) (ALVHH) Spire with shelves in southern portion of sheet flow (3 m). (i) (ALVBC) Looking along primary fissure (within a few hundred meters of Plate 3f) showing lava drainback sheets (5 m).

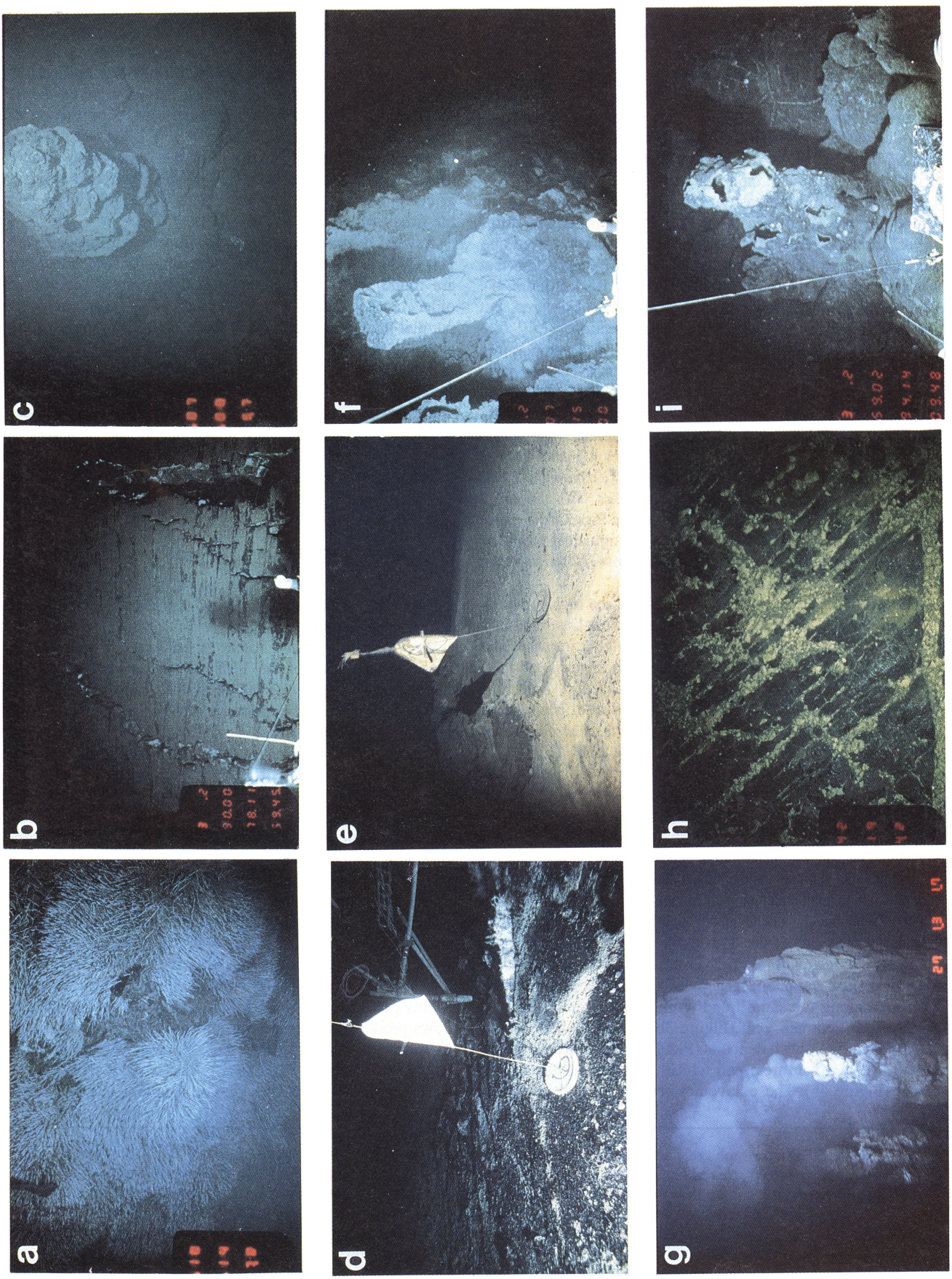
a
b
c
d
e
f
g
h
i

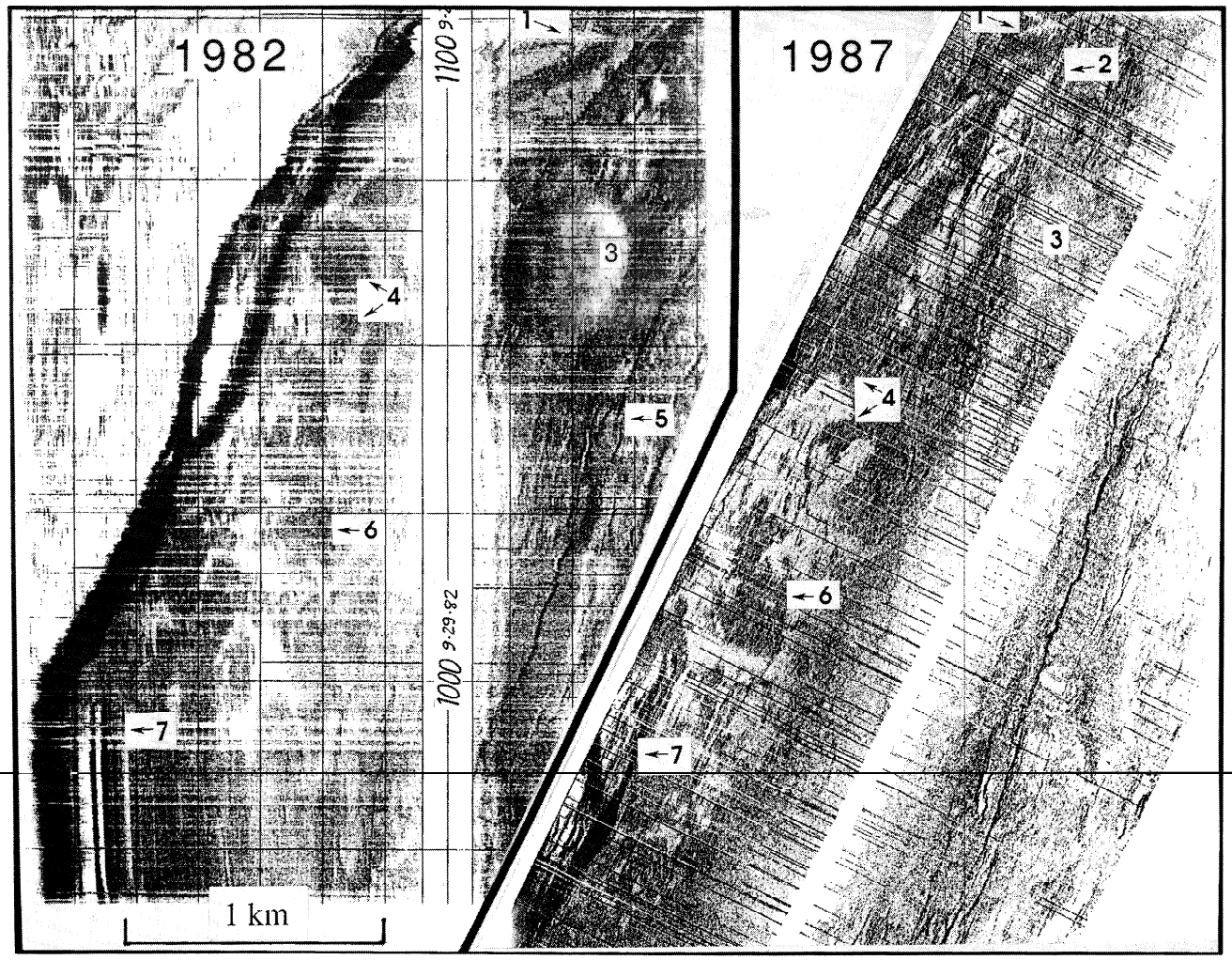

Figure 4. Comparison of 1982 and 1987 SeaMARC sidescan showing similar patterns of backscatter associated with sheet flow. Similar backscatter patterns are identified by number. The low backscatter (white) zones are areas of flat, lineated sheet flows. Note that the 1982 analogue record (no digital data available) is distorted by a large course change.

trend of the YSF lineations indicate that lava flowed from north to south, and the evidence for drainback into the northern part of the fissure system strongly points to the area between Cavern and Monolith as a primary eruptive vent area. However, submersible observations indicate that lava was also erupted from the fissure system as far south as 44°57′N.

The sheet flow covers about 3.5 km^2, but its thickness is not directly measurable. The volume of the sheet flow is 0.0035 km^3 for each meter of thickness, which means that it would have to be 14 m thick to equal the estimated total volume of the NPM (0.05 km^3 [*Chadwick and Embley*, this issue]). Submersible observations and topographic profiles

Plate 4. Photographs of vents at north Cleft site. Same abbreviations as Plate 3. (a) (TC) Luxuriant Vestimentiferan "bushes" at base of inner graben at 44°55′N site (8 m). (b) (ALVBC) Recent fissures (possibly small graben) at inner graben site (5 m). (c) (TC) Inactive sulfide chimney (~5–6 m high) located about 100 m east of line of most active venting (Plate 4). A few (apparently) alive Vestimentiferan were found at the base of the chimney during a subsequent *Alvin* dive. Sulfide samples taken here are composed mostly of pyrite and silica (6 m). (d) (ALVHH) Marker 6 at Tripod site, photo taken in September 1988. Note bare basalt and bacterial mats along fracture. (e) (ALVHH) Marker 6 at Tripod, photo taken in September 1991. Note extensive coating of iron-silica precipitate over previously bare basalt. This depositional event took place sometime between September 1988 and September 1990 (an *Alvin* dive in 1990 observed but did not obtain useable photographs) (3–4 m). (f) (ALVBC) Bacterial mats coating spires at edge of primary fissure. (g) (ALVHH) Organ pipe high-temperature vent. Tops of 5–6 m chimneys. (h) (TC) Extensive hydrothermal precipitate on young lineated sheet flows. (i) (ALVBC) Old sulfide chimney at contact between young sheet flow and older lobate flow. Chimney is hollow. Black coating is either lava spatter or manganese.

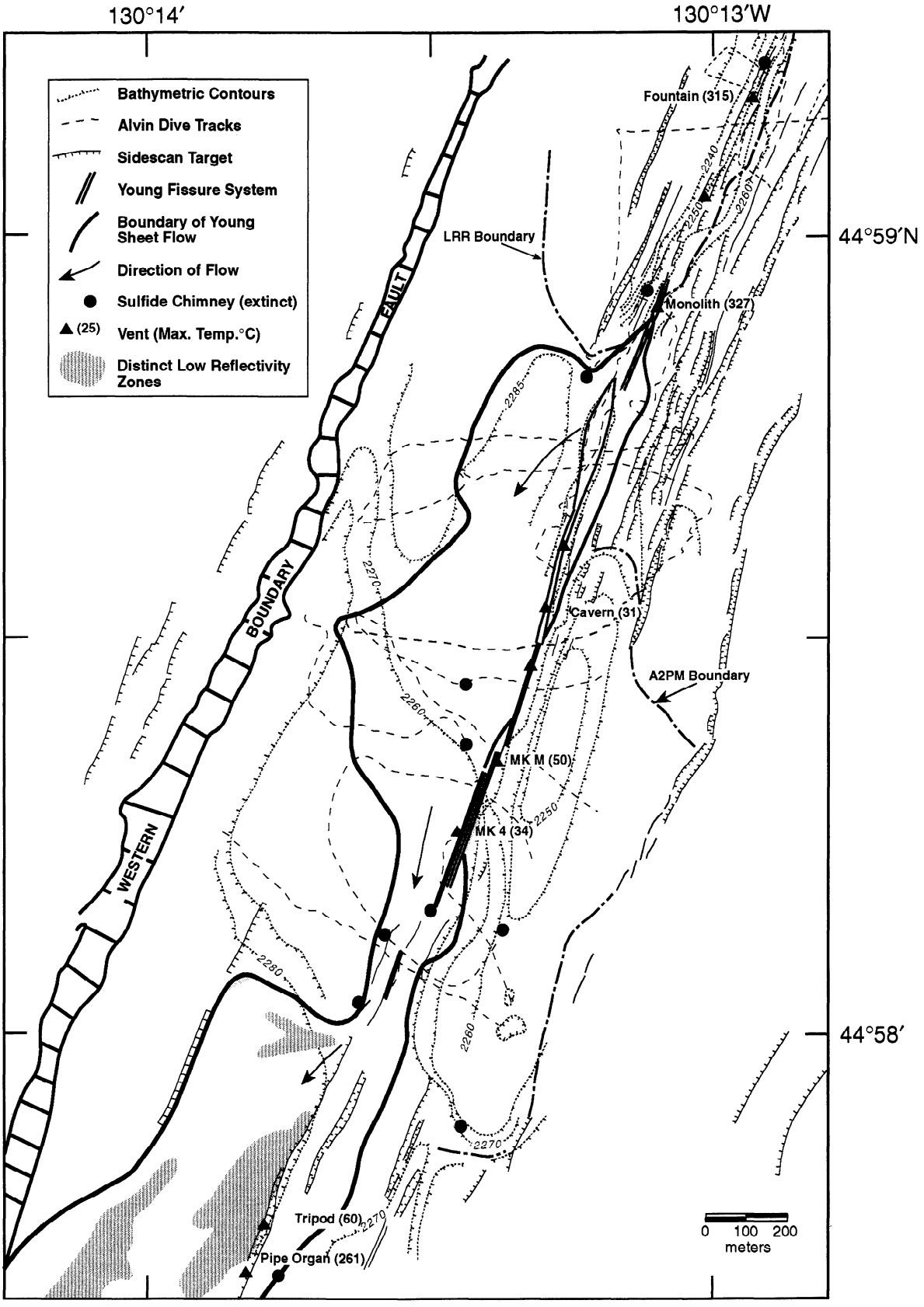

Figure 5a. Geology and bathymetry of northern part of sheet flow. Bathymetry is based on *Alvin* and towed camera pressure depth and altitude data. LRR is Lava Rise Ridge, A2PM is age 2 pillow mounds (age 1 is YSF and NPM). Most of the structural information is based on SeaMARC I sidescan imagery (Figure 5b, opposite). Western boundary fault is 80 to 100 m in relief.

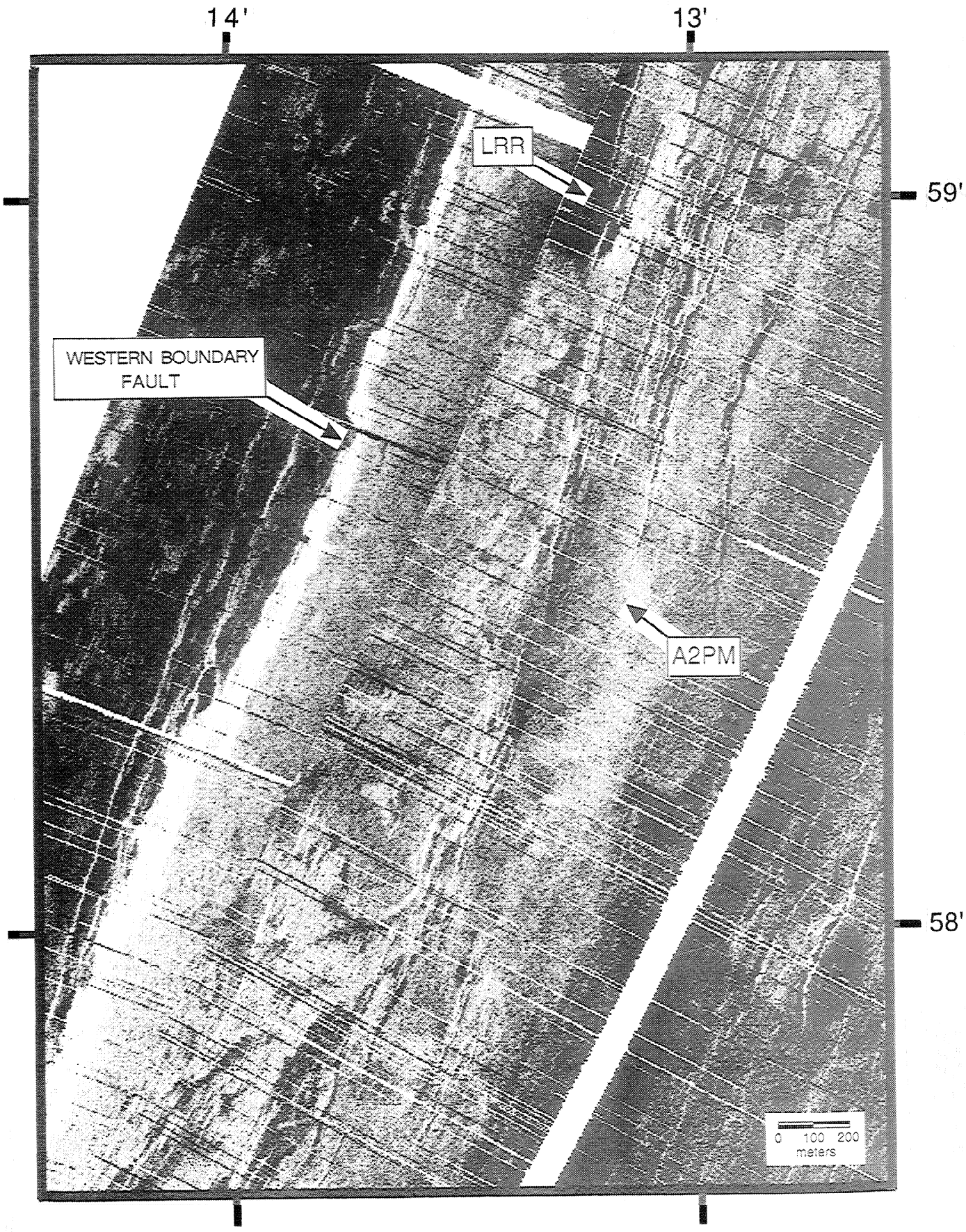

Figure 5b. Sidescan mosaic of same area as Figure 5a (opposite).

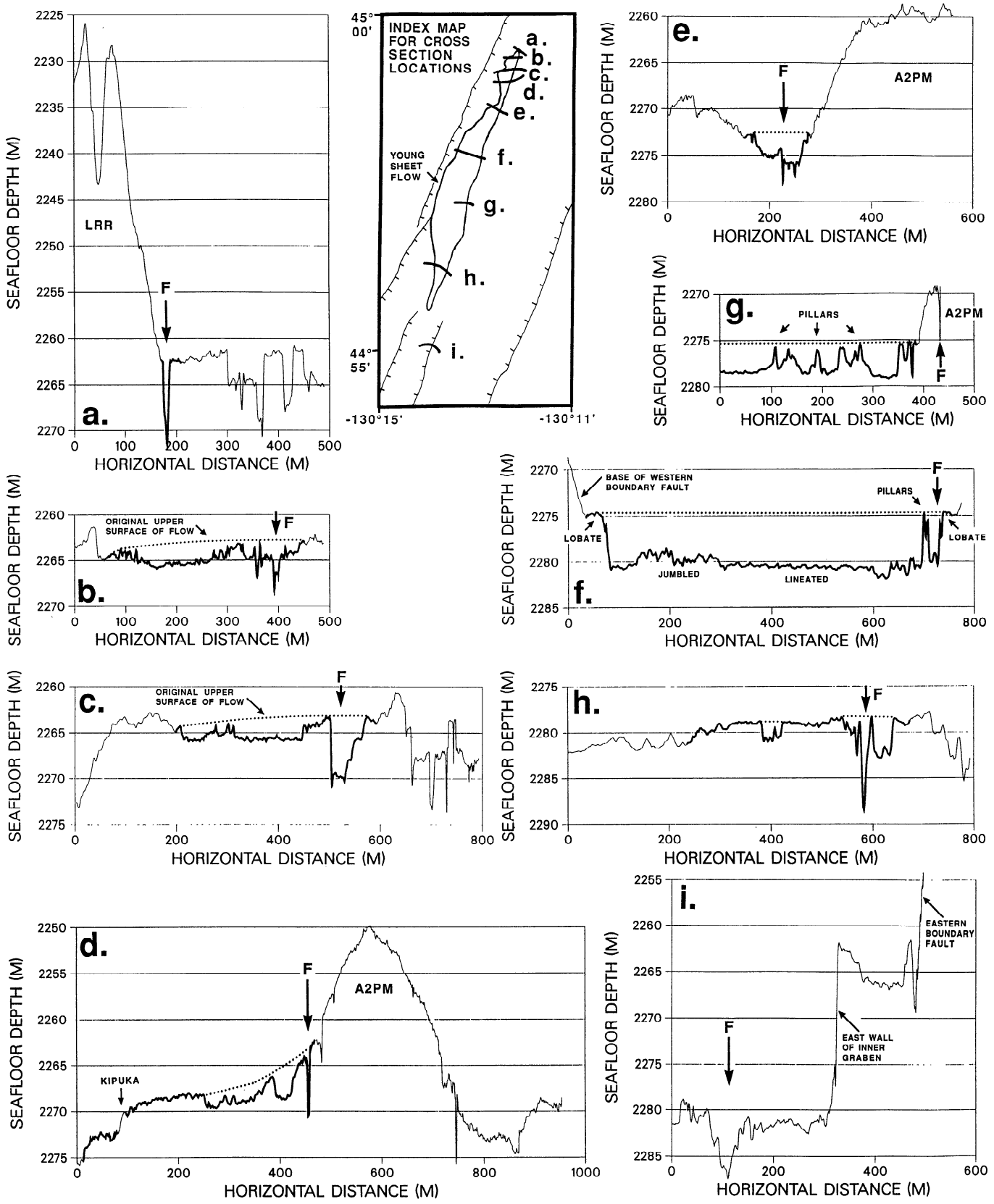

Figure 6. Cross sections of north Cleft segment using *Alvin* and towed camera microbathymetry. Bold thick line on cross sections show extent of YSF. F and arrow shows location of hydrothermal activity and/or most recently active fissure. A2PM is age 2 pillow mound. Locations of cross sections for Figures 8 and 9 in inset. Letters on inset map refer to following cross sections: (a) Camera tow 1989–14, (b) *Alvin* dive 2429, (c) *Alvin* dive 2269, (d) *Alvin* dive 2269, (e) *Alvin* dive 2267, (f) *Alvin* dive 2431, (g) *Alvin* dive 2444, (h) camera tow 1987–4, and (i) camera tow 1987–5.

(Figure 6) suggest that the YSF is probably no more than 5 m in thickness, making it of considerably less volume than the NPM.

The origin of lava pillars has been hypothesized to be from the trapping and superheating of water under a lava flow [*Francheteau et al.*, 1979], analogous to the formation of spiracles on marshy areas on land [*Waters*, 1960]. Observations of sheet flows along the Galapagos Rift [*Ballard et al.*, 1979] and the EPR [*Francheteau and Ballard*, 1983] suggested that pillars form within the margins of lava ponds or lakes, whereas the north Cleft pillars formed along the boundary of a moving flow, although it may have ponded temporarily as it advanced. Presumably, the YSF moved faster in the middle than at the edges, so the pillars only formed where water pockets were trapped and could rise up through the relatively stagnant edges of the flow. The lineated flows in the floors of collapsed areas mark the top of the subsided interior of the lava flow after the bulk of the flow had drained out to the south or back into the fissure.

Magma supply system: Clues from the pattern of hydrothermal activity. The eruptive fissure on the eastern side of the YSF is the locus of most of the hydrothermal venting along the northern Cleft segment. Water column data [*Embley et al.*, 1991; *Baker*, this issue] show that the northern limit of the hydrothermal plumes is at about 45°03′N. Towed camera and submersible data show only sporadic venting north of about 45°00′N and no active venting north of 45°04′N. The YPM are, in places, covered with thick pockets of yellow/orange sediments with some sulfide minerals [*Chadwick and Embley*, this issue], indicating some short-lived venting probably occurred immediately following the eruption. The most important point is that the NPM are characterized by a lack of hydrothermal venting relative to the YSF area even though the volume of extruded lava in the NPM is probably greater than the YSF.

One model to explain this pattern is that the YSF overlies a magma reservoir and that the NPM were fed by a lateral dike injection from the reservoir (Figure 7). The proposed magma body beneath the YSF is the heat source for the long-lived, high-temperature vents there, but only short-lived venting was associated with the dike intrusion beneath the NPM. Dikes of several meters width (typical of ophiolitic, and by inference, oceanic dikes) intruded into cold host rocks will "freeze" (cool to solidus temperature) within a few months [*Wilson and Head*, 1988]. Alternatively, the dike that fed the NPM eruption could have been injected vertically from below, but the lack of a long-lived (more than a few years) hydrothermal system implies that its magma source was either completely depleted by the eruption or is sealed off from transferring heat to the seafloor. We prefer the lateral dike injection model because it is supported by the body of evidence from the mid-ocean ridge system and from terrestrial volcanic systems for long-distance lateral dike injection within rift zones.

Iceland is one of the few portions of the mid-ocean ridge above sea level, and while it may be anomalous in some ways, it has helped illustrate important plate boundary processes. A well-monitored rifting episode occurred in northern Iceland between 1975 and 1984, and consisted of repeated lateral dike injections, basaltic fissure eruptions, and associated tectonic extension along the plate boundary [*Bjornsson et al.*, 1979; *Sigurdsson*, 1987]. During each of 20 discrete rifting events, magma from a reservoir beneath Krafla Caldera was injected into the rift zone and dikes were propagated for tens of kilometers. It is noteworthy that the along-axis gradients of the Krafla Rift Zone and the Cleft segment do not dramatically differ (Figure 2). Evidence for lateral dike injection is also commonly observed in Hawaii [*Rubin and Pollard*, 1987] and has recently been found within the Troodos ophiolite [*Staudigel et al.*, 1992]

In addition to the pattern of hydrothermal activity, the relationship between faults and fissures and volcanic vents supports the lateral dike injection model for the north Cleft segment. The NPM lie along an apparently continuous fissure/graben system (Figures 1 and 3 [*Chadwick and Embley*, this issue]) that is also along the same strike as the eruptive fissure of the YSF. Continuity of structures and their association with volcanic vents are all consistent with the lateral passage of dikes close to the seafloor [*Rubin*, 1992].

A detailed analysis of the Cleft segment lava chemistry data

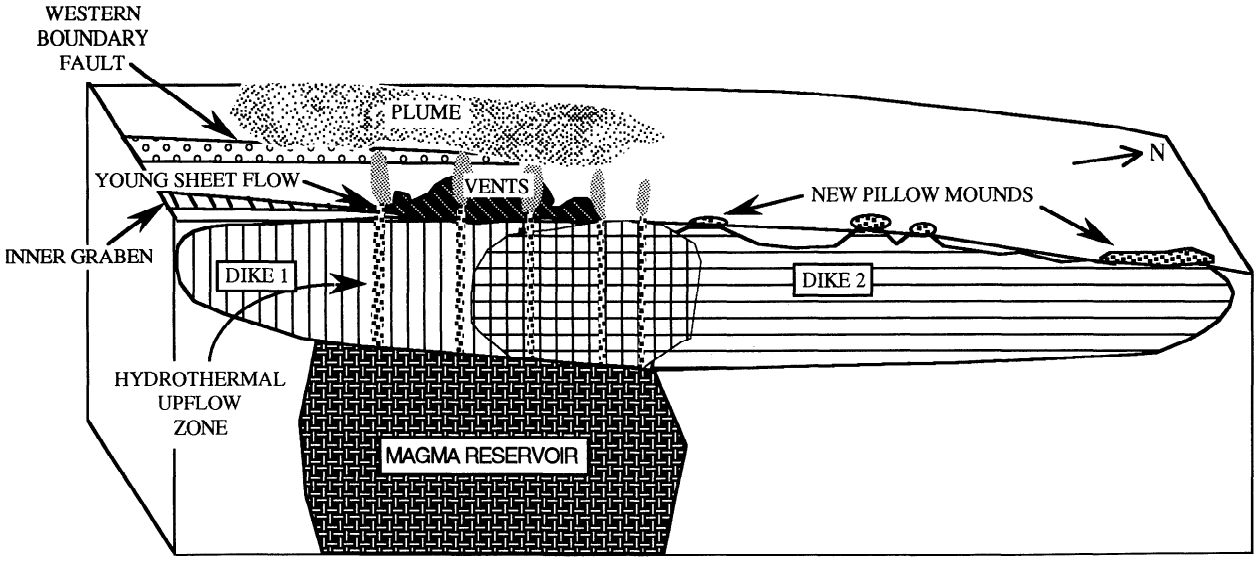

Figure 7. Cartoon of preferred model for Cleft 1980s intrusion/eruption episode(s) based on geologic and hydrothermal observations discussed in this paper. Sketch covers along-axis section from approximately 44°53′N to 45°10′N.

led *Smith et al.* [this issue] to conclude that the NPM and YSF lavas have slight, but significant chemical differences. The YSF lavas are relatively evolved and remarkably chemically homogeneous, whereas the NPM are more mafic and show more chemical diversity [*Smith et al.*, this issue]. The geochemical data are consistent with the idea that the NPM lavas were erupted after the YSF. The more primitive NPM magma apparently rose from a deeper level, mixed with the more differentiated and shallower YPM magma and then was intruded into the shallow oceanic crust.

Geophysical data are equivocal on the presence or absence of a small magma lens beneath the north Cleft segment. *Morton et al.* [1987] collected multichannel seismic reflection profiles over the Cleft segment and interpreted a faint reflector at a subbottom depth of 2.3–2.5 km to be the top of a partly solidified magma chamber. This reflector appears on cross sections beneath the Cleft axial valley at 44°40′N and the Vance axial valley at 45°05′N, but the only data from the YSF area (part of an along-axis profile) were not reprocessed to verify the presence of the reflector. Shallow seismic refraction data for the northern Cleft segment [*McDonald et al.*, this issue] are explained in terms of variations in layer 2A thickness, but a magma lens could be present below the limit (~500 m) of those measurements. Analysis of bottom gravity measurements reveals a possible low-density anomaly in the overlap region between the Cleft and Vance segments, which *Stevenson et al.* [this issue] interpret as a magma lens. In any case, the resolution of the available data is insufficient to precisely relate surface morphology and depth of magma lens (or absence thereof) to the hydrothermal vent distribution, such as *Haymon et al.* [1991] were able to do at the 9.5°N East Pacific Rise site.

The most likely cause of megaplume formation over the southern Juan de Fuca Ridge was the rifting associated with the NPM intrusion and eruption [*Baker et al.*, 1989; *Baker and Lupton*, 1990; *Embley et al.*, 1991]. Less clear is the extent of the rifting. No new lava has been observed along the southern Cleft segment during submersible dives made in the late 1980s and early 1990s, and *Baker* [this issue] does not report any major perturbations at the southern site during the annual along-axis CTD tows made since 1986. Therefore, even though the south Cleft segment is the shoalest part of the segment, it seems unlikely that the recent northern lavas can be attributed to along-strike dike injection originating on the southern end of the Cleft segment or that the two sites are underlain by a single magma chamber. Also, variations in lava chemistry along the Cleft segment [*Smith et al.*, this issue] strongly imply that separate melt lenses have fed the youngest flows at the northern and southern ends of the segment. Therefore the most recent spreading event may have been confined to the northern portion of the segment.

Baker [this issue] shows that the level of hydrothermal activity as measured in the integrated neutrally buoyant plume has been steadily decreasing since 1990. If this trend continues, one may conclude that the magma lens beneath the YSF area is relatively small and is cooling faster than it is being replenished or is being sealed off from the seafloor plumbing system. Continued monitoring of the plumes and vent fluids over the next several years will test this hypothesis. As this paper was in its final stages of revision in June 1993, a submarine rifting event was detected by a newly developed real-time monitoring system using the U.S. Navy's Sound Surveillance System (SOSUS). Swarms of seismic events occurring over several weeks were observed between 46°10′N and 46°35′N on the northern Juan de Fuca Ridge [*Fox*, 1993; *Dziak and Fox*, 1993]. This episode also generated megaplumes (albeit somewhat smaller than the 1986 megaplume) that formed over the site of a small volcanic eruption that took place during the seismic swarm period [*Embley et al.*, 1993]. This event appears to be analogous to the Cleft episode, and may provide an important step forward to a better understanding of the mechanism of crustal accretion at intermediate-rate spreading centers.

Conclusions

1. The northern Cleft segment has experienced two recent episodes of seafloor spreading. The extrusive activity associated with these episodes is bimodal; a sheet flow (high extrusion rate) probably erupted first, then at least 7 months later a more voluminous eruption of pillow lavas (slow extrusion rate) occurred along the northward extension of the same fissure system over a line extending 20 km to the north.

2. The eruptive fissure for the YSF is also the primary source of hydrothermal activity, a relationship that has also been observed at the southern Cleft segment. The YSF erupted along several kilometers of a fissure system, but its northernmost section appears to have been the longest-lived eruptive site. The lava pillars along the eastern and western margins of the YSF were probably formed along the slower moving margins of the flow and their tops preserve the original level of the upper flow surface before it drained out to the south. This eruption probably lasted only hours or days.

3. The suite of sulfide chimneys found within 100 m of the currently hydrothermally active fissure system indicates that there was a lower temperature, presheet flow hydrothermal system at the northern Cleft site.

4. The low level of hydrothermal activity over the NPM relative to the YSF and the continuity of rift structures connecting the volcanic vents suggest that the NPM were fed by a dike injected laterally to the north that subsequently cooled rapidly. There are some indications from plume measurements and bottom time series observations that the hydrothermal vents associated with the sheet flow area are also decreasing in intensity.

Acknowledgments. This work was supported through the NOAA Vents Program, and we thank Steve Hammond, the Vents Program manager, for his support through the course of this study. We are also particularly grateful to the NOAA Undersea Research Program and their Program Manager, David Duane, for support of the *Alvin* dive programs. Many persons contributed to the program at sea, but we particularly thank Susan Hanneman, Todd Schattgen, Dan Clapp, Bob Dziak, Kim Murphy, Bruce Appelgate, Roy Newman, Annette deCharon, Dennis Seem, Floyd Mader, and Andra Bobbitt. The skill and dedication of the Alvin Group should never be taken for granted, and we gratefully acknowledge their performance in providing a safe and effective research submersible. We thank the officers and crew of the research vessels *Atlantis II* and *Discoverer* for their dedication to deep-ocean research. Many colleagues contributed to various stages of this study, in particular, Ian Jonasson, Chris Fox, Gary Massoth, Mike Perfit, Dave Butterfield, Kim Murphy, Dick Feely, Ed Baker, Randy Koski, and Matt Smith. Finally, we thank Jessica Waddell for her attention to detail in editing the final manuscript. We thank Bill Normark, Ellen Kappel, and

Mike Perfit for their careful and constructive reviews of the manuscript. PMEL contribution 1429.

References

Appelgate, B. T., Volcanic and structural morphology of the south flank of Axial Volcano, Juan de Fuca Ridge: Results from a SeaMARC I side scan sonar survey, *J. Geophys. Res.*, *95*, 12,689–12,966, 1990.

Appelgate, B. T., and R. W. Embley, Submarine tumuli and inflated tube-fed lava flows on Axial Volcano, Juan de Fuca Ridge, *Bull. Volcanol.*, *54*, 447–458, 1992.

Baker, E. T., A 6-year time series of hydrothermal plumes over the Cleft segment of the Juan de Fuca Ridge, *J. Geophys. Res.*, this issue.

Baker, E. T., and J. E. Lupton, Changes in submarine hydrothermal ^{3}He/heat ratios as an indicator of magmatic/tectonic activity, *Nature*, *346*, 557–558, 1990.

Baker, E. T., G. J. Massoth, and R. A. Feely, Cataclysmic venting on the Juan de Fuca Ridge, *Nature*, *329*, 149–151, 1987.

Baker, E. T., W. Lavelle, R. A. Feely, G. J. Massoth, and S. L. Walker, Episodic venting on the Juan de Fuca Ridge, *J. Geophys. Res.*, *94*, 9237–9250, 1989.

Ballard, R. D., R. J. Holcomb, and T. H. van Andel, The Galapagos Rift at 86°W, 3, Sheet flows, collapse pits and lava lakes of the rift valleys, *J. Geophys. Res.*, *84*, 5407–5422, 1979.

Bjornsson, A., G. Johnsen, S. Sigurdsson, G. Thorbergsson, and E. Trygvasson, Rifting of the plate boundary in north Iceland 1975–1978, *J. Geophys. Res.*, *84*, 3029–3038, 1979.

Butterfield, D. A., and G. J. Massoth, Geochemistry of north Cleft segment vent fluids: Temporal changes in chlorinity and their possible relation to recent volcanism, *J. Geophys. Res.*, this issue.

Chadwick, W. W., Jr., and R. W. Embley, Lava flows from a mid-1980s submarine eruption on the Cleft segment, Juan de Fuca Ridge, *J. Geophys. Res.*, this issue.

Chadwick, W. W., Jr., R. W. Embley, and C. G. Fox, Evidence for volcanic eruptions on the southern Juan de Fuca Ridge between 1981 and 1987, *Nature*, *350*, 416–418, 1991.

de Moustier, C., and M. C. Kleinrock, Bathymetric artifacts in Sea Beam modeling of a propagating rift: Galapagos 95°30′W, *J. Geophys. Res.*, *91*, 3407–3424, 1986.

Dziak, R. P., and C. G. Fox, Seismo-acoustic evidence of a dike injection along the CoAxial segment, Juan de Fuca Ridge, *Eos Trans. AGU*, *74*, Fall Meeting suppl., 619, 1993.

Embley, R. W., S. R. Hammond, A. Malahoff, W. B. F. Ryan, K. Crane, and E. Kappel, Rifts of the southern Juan de Fuca, *Eos Trans. AGU*, *64*, 853, 1983.

Embley, R. W., W. W. Chadwick, and C. G. Fox, New evidence for volcanic eruptions on the southern Juan de Fuca Ridge during the 1980s—Implications for megaplumes and seafloor monitoring, *Eos Trans. AGU*, *71*, 1602, 1990a.

Embley, R. W., K. M. Murphy, and C. G. Fox, High-resolution studies of the summit of Axial Volcano, *J. Geophys. Res.*, *95*, 12,785–12,812, 1990b.

Embley, R. W., W. W. Chadwick, Jr., M. R. Perfit, and E. T. Baker, Geology of the northern Cleft segment, Juan de Fuca Ridge: Recent lava flows, sea-floor spreading, and the formation of megaplumes, *Geology*, *19*, 771–775, 1991.

Embley, R. W., W. W. Chadwick, Jr., I. R. Jonasson, S. Petersen, D. Butterfield, V. Tunnicliffe, and K. Juniper, Geological inferences from a response to the first remotely detected eruption at the mid-ocean ridge: CoAxial segment, Juan de Fuca Ridge, *Eos Trans. AGU*, *74*, Fall Meeting suppl., 619, 1993.

Fox, C. G., K. Murphy, and R. W. Embley, Automated display and statistical analysis of interpreted deep-sea bottom photographs, *Mar. Geol.*, *178*, 199–216, 1988.

Fox, C. G., W. W. Chadwick, Jr., and R. W. Embley, Detection of changes in ridge crest morphology using repeated multibeam sonar surveys, *J. Geophys. Res.*, *97*, 11,149–11,162, 1992.

Fox, C. G., Real-time detection of a volcanic eruption on the Juan de Fuca Ridge using the U.S. Navy Sound Surveillance System, *Eos. Trans. AGU*, *74*, Fall Meeting. suppl., 619, 1993.

Francheteau, J. T., and R. D. Ballard, The East Pacific Rise near 21°N, 13°N and 20°S: Inferences for along-strike variability of axial processes of the mid-ocean ridge, *Earth Planet. Sci. Lett.*, *64*, 93–116, 1983.

Francheteau, J. T., T. Juteau, and C. Rangan, Basaltic pillars in collapsed lava pools on the deep-ocean floor, *Nature*, *281*, 209–211, 1979.

Griffiths, R. W., and J. H. Fink, Solidification and morphology of submarine lavas: A dependence on extrusion rate, *J. Geophys. Res.*, *97*, 19,729–19,737, 1992.

Haymon, R. M., D. J. Fornari, M. H. Edwards, S. Carbotte, D. Wright, and K. C. MacDonald, Hydrothermal vent distribution along the East Pacific Rise crest (9°09′–54′N) and its relationship to magmatic and tectonic processes on fast-spreading mid-ocean ridges, *Earth Planet. Sci. Lett.*, *104*, 513–534, 1991.

Haymon, R. M., et al., Volcanic eruption of the mid-ocean ridge along the East Pacific Rise crest at 9°45–52′N, I, Direct submersible observations of seafloor phenomena associated with an eruption event in April 1991, *Earth Planet. Sci. Lett.*, *119*, 71–83, 1993.

Howard, K. J., and M. R. Fisk, Hydrothermal alumina-rich clays and boehmite on the Gorda Ridge, *Geochim. Cosmochim. Acta*, *52*, 2269–2279, 1988.

Humphris, S. E., W. B. Bryan, G. Thompson, and L. Autio, Morphology, geochemistry, and evolution of Serocki Volcano, *Proc. Ocean. Drill. Program, Sci. Results, 106/107*, 67–84, 1990.

Johnson, H. P., and M. Holmes, Evolution and plate tectonics: The Juan de Fuca Ridge, in The Geology of North America, vol. IV, The Eastern Pacific Ocean and Hawaii, edited by E. L. Winterer, D. M. Hussong, and R. W. Decker, pp. 73–91, Geological Society of America, Boulder, Colo., 1989.

Kappel, E. S., and W. R. Normark, Morphometric variability within the axial zone of the southern Juan de Fuca Ridge: Interpretation from SeaMARC II, SeaMARC I and deep-sea photography, *J. Geophys. Res.*, *92*, 11,291–11,302, 1987.

Kappel, E., and W. R. Normark, Results from camera tows along the southern Juan de Fuca Ridge: A2–84-WF, *U.S. Geol. Surv. Open File Rept.*, *88–371*, 1988.

Kappel, E. S., and W. B. F. Ryan, Volcanic episodicity and a non-steady state rift valley along northeast Pacific spreading centers: Evidence from SeaMARC I, *J. Geophys. Res.*, *91*, 13,925–13,940, 1986.

Koski, R. A., I. R. Jonasson, D. C. Kadko, V. K. Smith, and F. L. Wong, Compositions, growth mechanisms, and temporal relations of hydrothermal sulfide-sulfate-silica chimneys at the northern Cleft segment, Juan de Fuca Ridge, *J. Geophys. Res.*, this issue.

Macdonald, K. C., J. C. Sempere, and P. J. Fox, East Pacific Rise from Siqueiros to Orozco fracture zones: Along-strike continuity of axial neovolcanic zone and structure and evolution of overlapping spreading centers, *J. Geophys. Res.*, *89*, 6049–6069, 1984.

Macdonald, K. C., P. J. Fox, L. J. Perram, M. F. Eissen, R. M. Haymon, S. P. Miller, S. M. Carbotte, M. H. Cormier, and A. N. Shor, A new view of the mid-ocean ridge from behavior of ridge axis discontinuities, *Nature*, *335*, 217–225, 1988.

McDonald, M. A., J. A. Hildebrand, S. C. Webb, and C. Fox, Seismic structure and anisotropy of the Juan de Fuca Ridge at 45°N, *J. Geophys. Res.*, this issue.

Massoth, G., E. T. Baker, J. E. Lupton, R. A. Feely, D. A. Butterfield, K. L. Von Damm, K. K. Roe, and G. T. Lebon, Temporal and spatial variability of hydrothermal manganese and iron at the Cleft segment, Juan de Fuca Ridge, *J. Geophys. Res.*, this issue.

Milligan, B. N., and V. Tunnicliffe, Vent and nonvent faunas of Cleft segment, Juan de Fuca Ridge, and their relations to lava age, *J. Geophys. Res.*, this issue.

Morton, J., N. H. Sleep, W. R. Normark, and D. H. Tomkins, Structure of the southern Juan de Fuca Ridge from seismic reflection records, *J. Geophys. Res.*, *92*, 11,315–11,326, 1987.

Murphy, K. M., and R. W. Embley, A morphologic and structural study of the Vance Seamount Chain: Relationship to volcanism on the Juan de Fuca Ridge, *Eos Trans. AGU*, *69*, 1503, 1988.

Normark, W. R., J. L. Morton, R. A. Koski, and D. A. Clague, Active hydrothermal vents and sulfide deposits on the southern Juan de Fuca Ridge, *Geology*, *11*, 158–163, 1983.

Normark, W. R., J. L. Morton, and S. L. Ross, Submersible observations along the southern Juan de Fuca Ridge: 1984 *Alvin* Program, *J. Geophys. Res.*, *92*, 11,283–11,290, 1987.

Renard, V., and P. Allenou, SEA BEAM multi-beam echo sounding in "Jean-Charcot". Description, evaluation and first results, *Int. Hydrogr. Rev.*, *56*, 35–67, 1979.

Rubin, A. M., Dike-induced faulting and graben subsidence in volcanic rift zones, *J. Geophys. Res.*, *97*, 1839–1858, 1992.

Rubin, A. M., and D. D. Pollard, Origins of blade-like dikes in volcanic rift zones, in Volcanism in Hawaii, edited by R. W. Decker, T. L. Wright, and P. H. Stauffer, *U.S. Geol. Surv. Prof. Pap., 1350*, 1449–1470, 1987.

Sigurdsson, H., Dyke injection in Iceland: a review, in Mafic Dyke Swarms, edited by H. C. Halls and W. F. Fahrig, *Geol. Assoc. Can. Spec. Pap., 34*, 55–64, 1987.

Smith, M. C., M. R. Perfit, and I. R. Jonasson, Petrology and geochemistry of basalts from the southern Juan de Fuca Ridge: Controls on the spatial and temporal evolution of mid-ocean ridge basalt, *J. Geophys. Res.*, this issue.

Staudigel, H., J. Gee, L. Tauxe, and R. J. Varga, Shallow intrusive directions in the Troodos ophiolite: Anisotropy of magnetic susceptibility and structural data, *Geology, 20*, 841–844, 1992.

Stevenson, J. M., J. A. Hildebrand, M. A. Zumberge, and C. Fox, An ocean bottom gravity study of the southern Juan de Fuca Ridge, *J. Geophys. Res.*, this issue.

U.S. Geological Survey (USGS), Juan de Fuca Study Group, Submarine fissure eruptions and hydrothermal vents on the southern Juan de Fuca Ridge: Preliminary observations from the submersible *Alvin*, *Geology*, *14*, 823–827, 1986.

Walker, G. P. L., Structure, and origin by injection, of lava under surface crust, of tumuli, "lava rises," lava-rise pits," and "lava-inflation clefts" in Hawaii, *Bull. Volcanol.*, *53*, 546–558, 1991.

Waters, A. C., Determining direction of flow in basalts, *Am. J. Sci.*, *258-A*, 350–366, 1960.

Wilson, L., and J. W. Head, III, Nature of local magma storage zones and geometry of conduit systems below basaltic eruption sites: Pu'u 'O'o, Kilauea East Rift, Hawaii, example, *J. Geophys. Res.*, *93*, 14,785–14,792, 1988.

W. W. Chadwick, Jr., Oregon State University, CIMRS, Hatfield Marine Science Center, Newport, OR 97365-5258.

R. W. Embley, Ocean Environment Research Division, PMEL, NOAA, Hatfield Marine Science Center, 2115 SE OSU Drive, Newport, OR 97365-5258.

(Received December 21, 1992; revised July 14, 1993; accepted July 21, 1993.)